

A Theoretical Approach for Predicting Transient Air Temperature in an Intake Manifold Preheater for a Cai Engine

Sebahattin ÜNALAN¹, Saliha ÖZARSLAN¹, Bilge ALBAYRAK ÇEPER¹, Evrim ÖZRAHAT²

¹Department of Mechanical Engineering, Faculty of Engineering, Erciyes University, Kayseri, Türkiye

²Department of Biosystems Engineering, Faculty of Engineering and Architecture, Bozok University, Yozgat, Türkiye

This paper investigates the time dependent relationship between inlet and outlet temperatures of a new manifold system incorporated with an air preheater in a spark ignition engine for a desired controlled auto ignition. A three-dimensional numerical modeling of the preheater and manifold was performed with a CFD code. Two heaters with powers of 600 W were located in the preheater. The calculations were realized for the air velocities of 20, 30, 60 and 90 m/s at the manifold outlet. The initial medium temperatures were chosen as 258 K and 300 K for winter and summer design values for Kayseri, respectively. In order to predict the air outlet temperatures of the new system, a time dependent correlation was developed from the results of the numerical calculations. It's well known that the transient numerical and experimental studies take a long time to reach the solution and they are costly. However, this correlation made it possible to predict the outlet temperature of air without any numerical or experimental work.

Keywords: Time dependent correlation, air heater, controlled auto ignition, intake manifold

1. INTRODUCTION

Controlled Auto-Ignition (CAI) combustion, also known as Homogeneous Charge Compression Ignition (HCCI), is receiving increased attention for its potential to improve both the efficiency and emissions of internal combustion (IC) engines. The CAI combustion process involves the auto-ignition and subsequent simultaneous combustion of a premixed combustible charge [1].

CAI combustion is achieved by controlling the temperature, pressure, and composition of the fuel-air mixture so that it spontaneously ignites in the engine. This unique characteristic of CAI allows the combustion of very lean or diluted mixtures, resulting in low combustion temperatures that dramatically reduce the engine-out NO_x emissions. As it has no throttling losses, the part-load fuel economy of a gasoline engine can be improved significantly, thus allowing a four-stroke

gasoline engine to achieve a 20 percent reduction in fuel consumption [2].

Various methods have been used to achieve CAI (or HCCI) combustion, principally as follows:

1. Higher compression ratio
2. More auto-ignitable fuel
3. Recycling of burnt gases (EGR and/or trapped residuals)
4. Direct intake charge heating [3].

Higher compression ratio will assist fuel to auto ignite, but it leads to knocking combustion at higher load conditions, limiting the maximum power output of the engine. In this point, it can be said that some fuels, such as alcohol fuels have shown to be superior according to other fuels [4]. But a dual fuelled engine requires additional fuelling systems and adds more complexity to engine control, making them unsuited for automotive applications [1].

In order to achieve CAI combustion, it needs a more precise control of intake charge temperature. The charge temperature depends on intake air and fuel temperatures, EGR gas temperature and EGR rate. For the CAI combustion without EGR, intake air electrical heaters can provide a valuable help by controlling air temperature [5]. The use of an electrical heater at the inlet of manifold seems to be the better solution because it allows controlling more precisely intake temperature. In addition, electrical heaters present more durability and lower costs than other solutions [6]. Moreover, electrical heaters can be used in order to assist the cold starting of the engine, dispensing glow plugs, which are intrusive elements in the combustion chamber [6-9].

The implementation of HCCI combustion in direct injection diesel engines using early, multiple and late injection strategies is reviewed extensively in literature [10]. Governing factors in HCCI operations such as injector characteristics, injection pressure, piston bowl

geometry, compression ratio, intake charge temperature, exhaust gas recirculation (EGR) and supercharging or turbo charging are discussed in this review. The effects of design and operating parameters on HCCI diesel emissions, particularly NO_x and soot, are also investigated. For each of these parameters, the theories are discussed in conjunction with comparative evaluation of studies reported in the specialized literature [10]. It was shown that increasing intake charge temperature from 31°C to 54°C increased NO_x emissions linearly from approximately 10 ppm to 50 ppm when n-heptane fuel was combusted at fixed fuel delivery rate, engine speed and 30% EGR. Both unburned HC and CO were observed to be unaffected by intake temperature [11]. Experiments conducted on a HSDI diesel engine revealed that peak soot luminosity were markedly reduced when intake temperature decreased from 110°C to 30°C under a load condition of 3 bar IMEP. This was attributed to both lower soot temperatures and reduced soot formation. Nonetheless, in-cylinder soot luminosity was clearly observed even at 30°C which indicated that complete eradication of soot formation was difficult with typical fuel injection system parameters [12].

Although the CAI combustion technology can be applied to gasoline or diesel engines with various methods; in this paper we will focus on the application of CAI combustion to gasoline engines with the method of direct charge heating. The main components of intake systems are manifold and preheater. The numerical modeling of intake manifold was considered in literature. The geometry effects of two intake manifolds on the in-cylinder flows by two methods are studied numerically and experimentally. A three-dimensional numerical modeling of the turbulent in-cylinder flow through the two manifolds was undertaken. Simulation and experiments results confirmed the benefits of the optimized manifold geometry on the in-cylinder flow and engine performances [13]. A typical manifold design for a range of flow-rates and exit pressure drops was analyzed using computational fluid dynamics and an empirical technique. High flow-rates and exit pressure drops produce even flow distributions in the manifold branches, as expected. Lower flow rates and exit pressure drops produce less even distributions and indicate quantitative disparity between analysis techniques. This case study illustrates the use of calculation techniques to predict upstream airflow behavior for combustion equipment nominally relying on even flow distributions [14].

Based on the 1D simulation results, the intake manifold design is optimized using 3D Computational Fluid Dynamics (CFD) software under steady state condition. As a result of this 3D CFD analysis, the disproportionate flow of air inside the runners is identified and pressure inside the runner is also experimentally investigated on the engine test bench. From the investigation, it is identified that the pressure inside the runners are uniform and smoke level is also reduced for optimized inlet manifold design [15].

A 3D Simulation of a XU7 Engine Intake Manifold is presented and the results discussed. The effect of length of runners on the volumetric efficiency had been analyzed by 3D CFD model at different speeds. In the model with 20% extended runners, the volumetric efficiency increases at 3500 and 4500 rpm. According to the results of steady and unsteady simulations, some suggestions are recommended to improve the performance of this intake manifold [16]. In these manifold modeling studies, the preheater is not considered [13-16].

In the literature, there are limited intake air preheating studies. These limited studies are mostly based on the performance of HCCI combustion. In addition, experimental work concerning fuel economy and low pollutants emissions from internal combustion engines includes successive changes of each of the many parameters involved, which is very demanding in terms of money and time. Therefore, a theoretical correlation could provide a fast and inexpensive adequate way for describing details of combustion and pollutants formation processes in internal combustion engines. For this purpose, a preheater of intake air manifold was designed three-dimensional and manifold outlet temperature was investigated numerically. Towards the obtained results a correlation which is related with velocity, density of air and time was developed for predicting the air outlet temperature without experimental work.

2. PROBLEM DESCRIPTION AND NUMERICAL METHOD

2.1. Geometry of the problem

In this study, the main aim is to calculate the outlet temperature of the intake manifold of an SI engine. As a function of the operation, also it is aimed to analyze the relation between the air flow velocity, air density, inlet and outlet temperatures. For this purpose a three-dimensional numerical model was generated by the

GAMBIT and studied by the commercial computational fluid dynamics software ANSYS FLUENT Version 15 [17]. Three-dimensional geometry of the manifold and preheater with real dimensions was created by SOLIDWORKS [18]. The files created by SOLIDWORKS were imported to GAMBIT to build the grid and then imported to FLUENT for the final calculation of simulation. The geometry and mesh of the model can be seen in Figure.1. The model consists of 15099226 fluid and 1708770 solid cells with total cells of 16807996. In this point, it should be noted that the very thin fins in the heater (thickness 0.1 mm, see Fig.2) requires a lot of mesh.

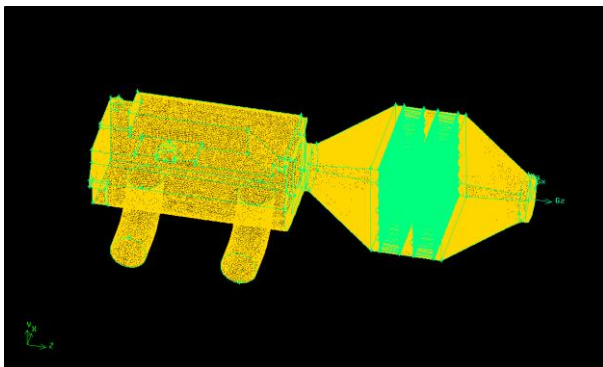
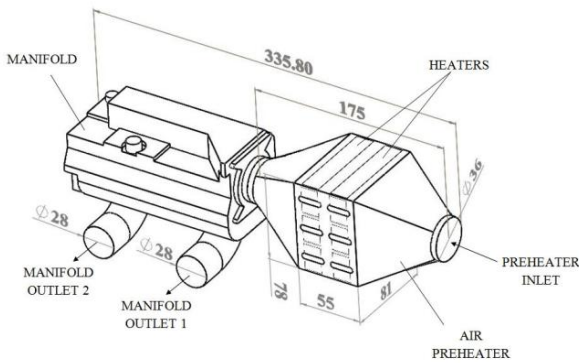


Figure 1: Geometry and mesh of the intake manifold and preheater model.

2.2. Main flow and energy equations

A three-dimensional transient, forced turbulent flow and conjugate heat transfer in the intake manifold and preheater with air flow inside was considered here. Under these conditions, the governing equations for continuity and momentum are presented below. The equation for continuity can be written as follows:

$$\frac{\partial \rho}{\partial t} + \nabla(\rho \bar{v}) = 0 \quad (1)$$

Momentum:

$$\frac{\partial}{\partial t}(\rho \bar{v}) + \nabla(\rho \bar{v} \bar{v}) = -\nabla p + \nabla(\mu \nabla \bar{v}) \quad (2)$$

Energy equation for fluid is as follows:

$$\frac{\partial}{\partial t}(\rho E) + \nabla(\bar{v}(\rho E + p)) = \nabla(k \nabla T) \quad (3)$$

In equation (3) E is:

$$E = h + \frac{p}{\rho} + \frac{v^2}{2} \quad (4)$$

where h is sensible enthalpy and calculated

$$\text{from } h = \int_{T_{ref}}^T c_p dT. T_{ref} \text{ is } 298.15 \text{ K for the}$$

pressure-based solver. Energy equation for solid is as follows:

$$\frac{\partial}{\partial t}(\rho h) + \nabla(\bar{v} \rho h) = \nabla(k \nabla T) \quad (5)$$

The governing equations are solved by the control volume approach using computational fluid dynamics software ANSYS FLUENT version 15. The governing equations are discretized using a second-order upwind scheme. The most widely used and validated model is the (k-ε) model for modeling the turbulence in flow. Therefore, in the present analysis, the (k-ε) model has been adopted. The problem is solved by using two additional equations. The k-ε realizable model uses the transport equations of k and ε to compute the turbulent viscosity. The modeled transport equations for k and ε in the realizable k-ε model are:

$$\frac{\partial}{\partial t}(\rho k) + \frac{\partial}{\partial x_j}(\rho k u_j) = \frac{\partial}{\partial x_j} \left[\left(\mu + \frac{\mu_t}{\sigma_k} \right) \frac{\partial k}{\partial x_j} \right] + G_k + G_b - \rho \epsilon \quad (6)$$

and

$$\frac{\partial}{\partial t}(\rho \epsilon) + \frac{\partial}{\partial x_j}(\rho \epsilon u_j) = \frac{\partial}{\partial x_j} \left[\left(\mu + \frac{\mu_t}{\sigma_\epsilon} \right) \frac{\partial \epsilon}{\partial x_j} \right] - \rho C_2 \frac{\epsilon^2}{k + \sqrt{v \epsilon}} + C_{1\epsilon} \frac{\epsilon}{k} C_{3\epsilon} G_b \quad (7)$$

In these equations, G_k represents the generation of turbulence kinetic energy due to the mean velocity gradients; G_b is the generation of turbulence kinetic energy due to buoyancy. For the realizable k-ε model, the default value of Pr is 0.85. σ_k and σ_ϵ are the turbulent Prandtl numbers for k and ε, respectively. The model constants in Eq.(7) are $C_{1\epsilon}=1.44$, $C_2=1.9$, $\sigma_k=1.0$, $\sigma_\epsilon=1.2$.

Simulations are carried out for time step of 0.1 s. For each time step, convergence criteria of governing equations were set to 10^{-4} . Transient computations are carried out for long enough time to ensure the energy balance.

2.3. Boundary Conditions

The system is modeled as a whole geometry consists of preheater and manifold. Adiabatic boundary conditions are applied at all external surfaces of preheater and

manifold. As seen in Fig.1, there are two heaters of 600 W per each one located in the midpoint of the preheater. The heaters are defined as internal heat source terms with a value corresponding to total 1200 W. The heaters commercially available from the market are selected as seen in Figure 2. In the numerical calculations, it assumed that the heater is made of aluminum. The specific heat, density and thermal conductivity of aluminum is taken from FLUENT database as 871 J/kgK, 2719 Kg/m³ and 202.4 W/mK, respectively.

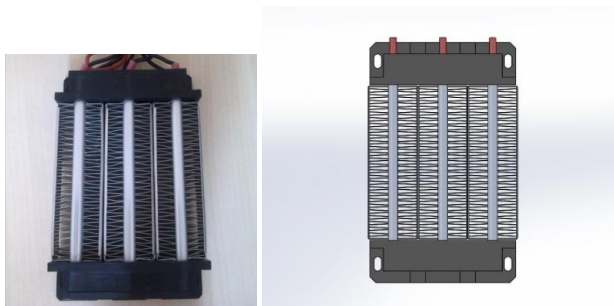


Figure 2: The heater and heater's model in SOLIDWORKS

Density of air is treated with the ideal gas law. Calculated specifications of specific heat (C_p), viscosity (μ) and thermal conductivity (k) of air is considered as a function of temperature, and described as a polynomial ($=A+BT+CT^2+DT^3+ET^4+FT^5$, $T>200$ K and $T<2300$ K with a deviation of maximum 2%) in Table 1.

Table 1: Calculated coefficients for equations of k , C_p and μ as a function of temperature

	A	B	C	D	E	F
k	-	-	-	-	-	-
[W/mK]	1,3080	1,9476	2,6613	2,2777	9.0668	1,4190
C_p	6.10^{-2}	9.10^{-4}	4.10^{-7}	3.10^{-10}	5.10^{-14}	7.10^{-17}
[J/kgK]	1,0466	0,3797	1,0297	7,7570	2,4272	2,3309.
μ	$.10^3$	3	1.10^{-3}	7.10^{-7}	9.10^{-10}	10^{-14}
[Kg/ms]	1,8714	7,7997	6,2354	3,5071	8,9768	8,0204
	6.10^{-7}	5.10^{-8}	1.10^{-11}	3.10^{-14}	9.10^{-18}	2.10^{-22}

The atmospheric pressure is determined as P_{atm} 89322 Pa for Kayseri corresponding to altitude of 1050 m. In the heater+manifold system as seen in Fig.1, the airflow will be provided by piston movement. At the intake time, sucked air into the cylinder will come to cylinder as heated by passing through the heater+manifold. Thus, at the first stage of analysis, the suction speed boundary condition is defined at the manifold outlet and pressure boundary condition is defined at the heater input. Piston speed depending on the crank

angular speed can be defined by the following equation:

$$V_p(t) = R\omega \left(\sin(\omega t) + \frac{R\sin(\omega t)\sin(\omega t)}{\sqrt{L^2 - (R\sin(\omega t))^2}} \right) \quad (8)$$

where ω is angular speed of the crank and calculated by $\omega = \frac{2\pi n}{60}$ depending on crankshaft (n [rpm]). R is the crank radius and L is rod length. The air velocity at the manifold outlet can be calculated depending on the piston speed:

$$V_m(t) = \left(\frac{D_p}{D_m} \right)^2 V_p(t) \quad (9)$$

where, D_p and D_m are piston diameter and manifold outlet diameter, respectively. From the equations; it is very clear that the air velocity in the manifold outlet changes over time. From Eqs.8 and 9, if the calculation is performed for the speed of the crankshaft ($2\pi = \omega t$), it can be seen that one tour is completed at 0.03 second for $n = 2000$. At the about half of 0.03 seconds, air flow will not be occurred due to compression-expansion and exhaust processes. At the other half, approximately 0.015 s, it will be seen that the air velocity values are changing in the between 0 and 45 m/s. For a correct approach in numerical calculations, this short period of time should be divided into numerous time intervals. Otherwise, the sudden rise of velocity and again down to zero at a very short time will bring computing challenges. The trials were unsuccessful in the heater, meshing the large number of fins with 0.1 mm thickness with enough aspect ratio led the formation of a lot of elements (cells of 16807996). The obligation of computation of this numerous number of cells with numerous time intervals caused long calculating time such as months with our computers. Therefore, the transient velocity at the manifold outlet is assumed as a constant value by computing the average values over suction period by the above equations. In the calculations, the average velocity values (V_i) at the heater inlet (inlet diameter $D_i = 0.036$ m) which are corresponding to the calculated average velocity values at the manifold outlet are estimated. V_i value is used as velocity inlet boundary condition in FLUENT. The calculated velocity values at possible speeds (900-4500 rpm) are given in Table 2. For the steady state case, the pressure loss on the heater-manifold system is calculated by using these pressure loss values, the heater pressure drop coefficient (K) of the system is determined by Eq.10. Heater is not operated in the

calculations made for the formation of Table 2. These results will assist in the calculation of the vacuum pressure in the cylinder.

Table 2: Results of pre-calculations

V_i [m/s]	V_m [m/s]	ΔP [Pa]	K
5	8.3229	112.01	3.234
10	16.629	430.74	3.115
20	33.255	1680.20	3.038
30	49.886	3744	3.009
40	66.512	6628	2.996
50	83.316	10316	2.972
60	99.759	14801	2.974

According to the calculations given in Table 2, it was seen that there is a significant pressure difference between inlet and outlet of the system. At the same time, the pressure loss coefficient is about 3.0 for all crank cycles

In Table 2, the pressure loss in the preheater and manifold (ΔP) and heater pressure drop coefficient (K) is calculated from the following equations for different velocity inlet values (V_i):

$$\Delta P = \frac{1}{2} K \rho V_m^2 \quad (10)$$

where ρ and V_m is air density and manifold outlet velocity, respectively.

In the second stage of the calculations, time-dependent calculations are performed. In these calculations, the heaters with 1200 W power were run and the air temperature of manifold outlet has been followed. For these calculations, velocity inlet boundary condition at the manifold outlet is applied as negative constant velocity (corresponding to velocities in Table-2) to achieve an accurate boundary condition. Thus vacuum pressure is obtained by applying negative velocity. The preheater inlet is chosen as pressure inlet at the atmospheric pressure. The initial temperatures of the air, heater and manifold are chosen as 258 K and 300 K for winter and summer design values for Kayseri, respectively.

3. RESULTS AND DISCUSSION

The numerical calculations are performed for $V_m=20, 30, 60$ and 90 m/s air flow velocities at the manifold outlet for a time period of 150 s. Calculations are realized for both winter and summer conditions. The initial temperatures of the system and air are assumed as 258 K and 300 K that Kayseri city are winter and summer design temperatures. The velocity and temperature contours at the end of 150 s can be seen in

Figure 3 and Figure 4. As can be seen from the figures, from two outlets on the manifold only one of them is assumed as outlet (on the left in the figures).

It can be said that the most important result obtained from Fig.3 is that when the inlet velocity of the system increases, a lower velocity region occurs at the upper part of the manifold outlet cross section according to the lower part. This can be explained by that the manifold outlet channel is a 90 degrees elbow.

According to the Fig.4, with increasing flow velocity and thus increasing crankshaft speed the air temperature at the manifold outlet decreases. This expected case will be important in terms of CAI combustion in the cylinder. Therefore, how the manifold outlet air temperature (T_{out}) changing over time is discussed in more detail in the following section.

The results of the numerical simulation for T_{out} values versus operation time can be seen in Figure 5. As seen in the figure, T_{out} values increases by increasing the operation time. This increase is going on until the steady-state condition. Then, the temperature curve reached a saturation value with increasing operation time. The time needed to reach this saturation value is lower for high velocity and higher for low velocity. For $V_m=90$ m/s, it takes 30 seconds and for $V_m=20$ m/s it takes 150 seconds to reach the saturation value.

From the numerical calculations in Fig.5, it was easily seen that there is a relationship between T_{out} , the initial temperatures (design temperatures), the saturation temperatures, operation time, air densities and air flow velocity values. Thereby, the curve characteristic in Fig.5 can be explained by the following equation analytically:

$$T_{out}(t) = a - be^{-ct} \quad (11)$$

where a, b and c are constants. At initial ($t = 0$), T_{out} should be equal to design temperature (T_{min}). If the system works for a long time ($t \rightarrow \infty$) temperature value should reach to saturation value (T_{max}). According to these two criterions, it can be easily determined that $a = T_{max}$ and $b = T_{max} - T_{min}$. By making some trial and error it is determined that the value of c constant vary as $c \sqrt{\rho A}$ depending on air density and flow velocity. Therefore, a new correlation for the T_{out} value can be explained as a function of the initial temperatures (design temperatures), the saturation temperatures, operation

time, air densities and air flow velocity values as follows:

$$T_{out}(t) = T_{max} - (T_{max} - T_{min})e^{-t\sqrt{\rho}A} \quad (12)$$

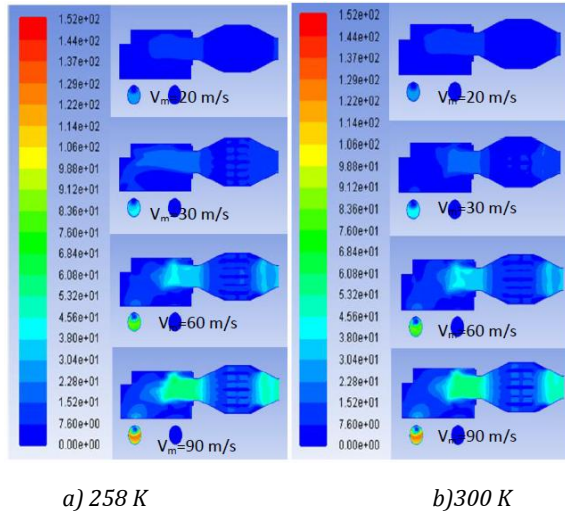


Figure 3: Velocity contours of air for different air flow velocities at the end of 150 s.

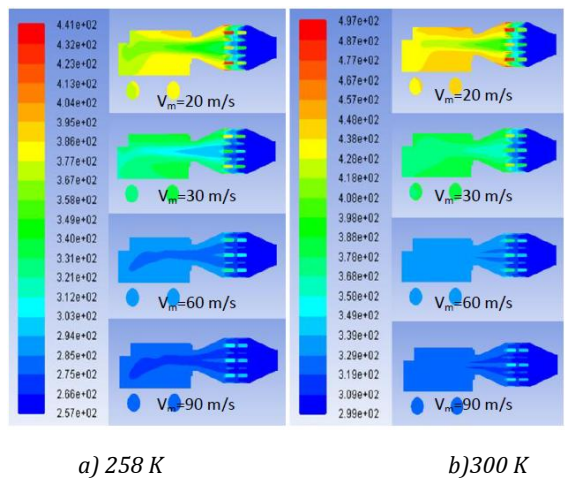


Figure 4: Temperature contours of air for different air flow velocities at the end of 150 s.

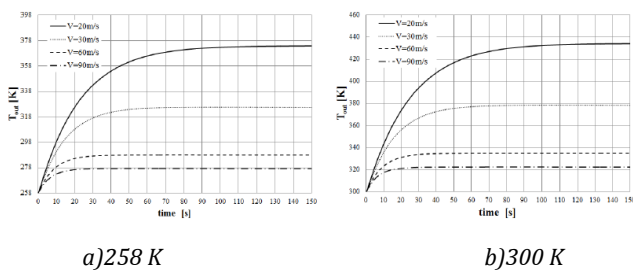


Figure 5: T_{out} values calculated from numerical calculations versus operation time for winter (a) and summer (b) conditions.

Where T_{min} is the design temperature, t is the operation time, ρ is the density of air at design temperature (from the ideal gas law), T_{max} is the saturation temperature

value at the manifold outlet. The coefficient A values calculated by curve fitting methods for different velocities are summarized in Table 3. Also variation of A values versus the velocity values are given in Figure 6.

Table 3: A values for different velocities

V_m [m/s]	10	20	30	60	90
A	0,0115	0,039	0,063	0,108	0,134

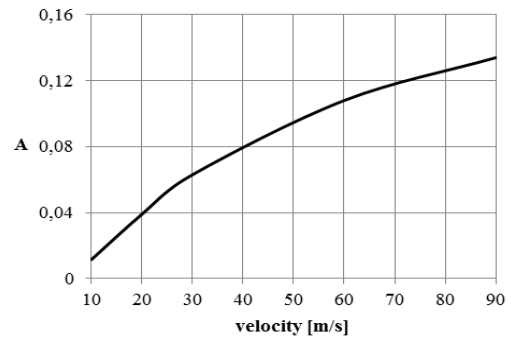
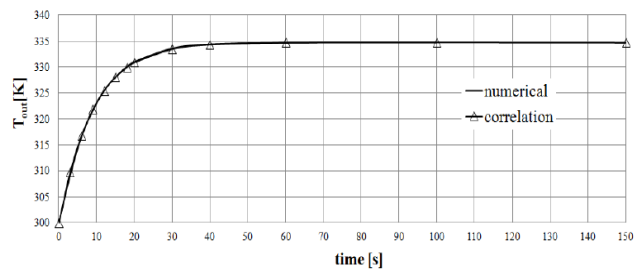
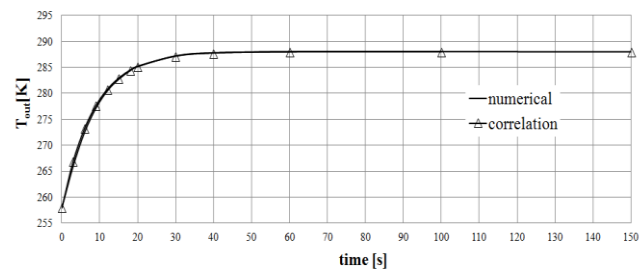


Figure 6: Variation of A values versus velocities.



a) 258 K



b) 300 K

Figure 7: T_{out} values calculated from numerical calculations and correlation versus operation time for $V=60$ m/s for winter (a) and summer (b) conditions.

For the practical use of the above correlation T_{max} value should be computable. When the saturation case is obtained in Fig.5, all of the heat produced will be given to flowing air. In this case, the following energy balance and equations can be written:

$$N = \frac{\pi}{4} CP(D_m^2 \rho_{out} V_m T_{max} - D_i^2 \rho_{atm} V_i T_{min}) \quad (13)$$

$$V_i = \left(\frac{D_m}{D_i}\right)^2 \frac{\rho_{out}}{\rho_{atm}} V_m \quad (14)$$

$$\rho_{out} = \frac{P_{atm}}{RT_{max}} \quad (15)$$

$$\rho_{atm} = \frac{P_{atm}}{RT_{min}} \quad (16)$$

If the above equations are rearranged and T_{max} value is extracted then the following equation is obtained:

$$T_{max} = \frac{\frac{\pi D_m^2}{4} P_{atm} V_m C_P}{\frac{\pi D_m^2}{4} P_{atm} V_m C_P - N R} T_{min} \quad (17)$$

where R is gas constant for air, C_P is the specific heat of air at the design temperature, N is the total heat power of the heaters.

This correlation showed an excellent performance as seen in Figure 7. For the brevity of the article the results only for $V_{out}=60$ m/s is given. For all velocity values the same harmony is captured. The difference between the T_{out} values calculated from numerical analyses and from the correlation is defined as ΔT . The ΔT values for winter condition ($T_{min}=258$ K) and summer condition ($T_{min}=300$ K) can be seen in Figure 8. Maximum error occurs as 0.9 K at the time of 3 s. However it is lower at the end of 150 s.

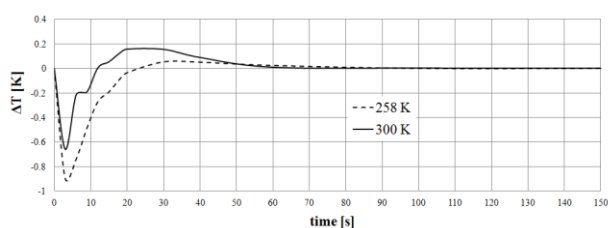


Figure 8: Variation of ΔT versus operation time for $V=60$ m/s

4. CONCLUSIONS AND RECOMMENDATIONS

In this paper, time dependent relationship between inlet and outlet temperatures of a new manifold system incorporated with an air preheater in a spark ignition engine for a desired controlled auto ignition was investigated. A three-dimensional geometry of the manifold and preheater was created with real dimensions. The preheater was designed by authors and the heaters were modeled with real dimensions according to a heater with a capacity of 600 W.

The three-dimensional steady state and transient analyses were performed by FLUENT. The temperature

distribution was obtained numerically for different air outlet temperatures and various air flow velocities. A correlation that is applicable to each kind of manifold was developed to predict the manifold outlet temperature of air as a function of the operation time.

ACKNOWLEDGMENT

The authors of this paper would like to acknowledge the financial support provided by TUBITAK Turkey under contract number 113M101 is gratefully acknowledged.

Nomenclature

A	correlation coefficient
BSFC	brake specific fuel consumption
C_p	specific heat (Joule.kg ⁻¹ K ⁻¹)
CA	crank angle
CAI	controlled auto ignition
CI	compression ignition
CO	carbon monoxide
CO ₂	carbon dioxide
CFD	computational fluid dynamics
D	diameter (m)
DI-HCCI	direct injection homogeneous charge compression ignition
E	energy (Joule)
EGR	exhaust gas recirculation
h	enthalpy
HC	hydrocarbon
HCCI	homogeneous charge compression ignition
H ₂ O	water
HSDI	high speed direct injection
IMEP	indicated mean effective pressure
k	turbulence kinetic energy (Joule/kg)
L	rod length (m)
N	total heat power of heaters
NO	nitric oxide
NO ₂	nitrogen dioxides
NO _x	nitrogen oxides
P	pressure

R	crank radius (m)
rpm	revolutions per minute
SI	spark ignition
T	temperature (K)
t	time (s)
V	velocity (m/s)
w	angular speed (rpm)
ρ	density (kg/m ³)
ε	turbulence dissipation rate (Joule kg ⁻¹ s ⁻¹)
μ	viscosity (kg m ⁻¹ s ⁻¹)

REFERENCES

- [1] Zhao H, Li J, Ma T, Ladommatos N. Performance and analysis of a 4-stroke multi-cylinder gasoline engine with CAI combustion. SAE 2002-01-0420; 2002.
- [2] Oakley A, Zhao H, Ladommatos N. Experimental studies on controlled auto-ignition (CAI) combustion of gasoline in a 4-stroke engine. SAE paper 2001-01-1030, 2001.
- [3] Kalian N, Zhao H, Qiao J. Investigation of transition between spark ignition and controlled auto-ignition combustion in a V6 direct-injection engine with cam profile switching. J. Automobile Engineering, 2008;222;1911-26.
- [4] Oakley A, Zhao H, Ma T, and Ladommatos N. Dilution Effects on the Controlled Auto-Ignition (CAI) Combustion of Hydrocarbon and Alcohol Fuels, SAE Paper 2001-01-3606.
- [5] Broatch A, Luján J.M., Serrano J.R., Pla B. A procedure to reduce pollutant gases from Diesel combustion during European MVEG-A cycle by using electrical intake air-heaters. Fuel, 2008; 87; 2760-78.
- [6] Payri F, Broatch A, Serrano JR, Rodríguez LF, Esmorís A. Study of the potential of intake air heating in automotive DI diesel engines. SAE paper 2006-01-1233; 2006.
- [7] Cooper B, Jackson N, Penny I, Rawlins D, Truscott A, Seabrook J. Advanced combustion system design, control and optimisation to meet the requirements of future European passenger cars. In: THIESEL 2004 conference on thermo-and fluid dynamic processes in diesel engines; 2004.
- [8] Mertz Rolf. Electric intake air heating for small and medium-sized diesel engines. MTZ MotortechnischeZeitschrift 1997;58.
- [9] Lindl Bruno, Schmitz Heinz-Georg. Cold start equipment for diesel injection engines. SAE paper 1999-01-1244; 1999.
- [10] Gan S., Ng HK, Pang KM. Homogeneous charge compression ignition (HCCI) combustion: implementation and effects on pollutants in direct injection diesel engines. Apply Energy, 2011;88:559-67.
- [11] Lü X, Chen W, Huang Z. A fundamental study on the control of the HCCI combustion and emissions by fuel design concept combined with controllable EGR. Part 2.Effect of operating conditions and EGR on HCCI combustion. Fuel 2005;84:1084-92.
- [12] Choi D, Miles PC, Yun H, Reitz RD. A parametric study of low-temperature, late - injection combustion in an HSDI diesel engine. JSME Series B 2005;48(4):656-64.
- [13] Jemni M.A., Kantchev G., Abid M.S. Influence of intake manifold design on in-cylinder flow and engine performances in a bus diesel engine converted to LPG gas fuelled, using CFD analyses and experimental investigations. Energy, 2011;36;2701-15.
- [14] Green A.S, Moutziz T. Case study: use of inlet manifold design techniques for combustion applications. Applied Thermal Engineering, 2002;22;1519-27.
- [15] Karthikeyan S, Hariganesh R, Sathyanadan M, Krishnan S, Vadivel P, Vamsidhar D. Computational analysis of intake manifold design and experimental investigation on diesel engine for lcv. International Journal of Engineering Science and Technology (IJEST), 2011;3;2359-67.
- [16] Maftouni N, Ebrahimi R. Intake manifold optimization by using 3-DCFD analysis with observing the effect of length of runners on volumetric efficiency. Proceedings of the 3rd BSME-ASME International Conference on Thermal Engineering, 20-22 December, 2006, Dhaka, Bangladesh.
- [17] ANSYS Inc. PDF Documentation for Release 15.0
- [18] SolidWorks 2014 Reference Guide by David C. Planchard